AIAA JOURNAL
Vol. 48, No. 2, February 2010

New Interference Approach for Ballistic Impact into Stacked Flexible Composite Body Armor

S. Leigh Phoenix* and A. Kadir Yavuz†
Cornell University, Ithaca, New York 14853
and
Pankaj K. Porwal‡
Indian Institute of Technology, Mumbai 400 076, India

DOI: 10.2514/1.45362

In this study a new interference model is developed to investigate the ballistic response of a hybrid, two-layered, flexible body armor. Because the stacking order of layers, which have distinctly different mechanical properties, has a large effect on the V_{50} limit velocity for penetration, we apply the analysis to a two-layer system consisting of fabrics of aramid (Kevlar29®) fiber and of ultrahigh molecular weight and drawn polyethylene (Dyneema®) fibers. Using right-circular cylindrical projectiles, previous experimental results of Cunniff ("An Analysis of the System Effects in Woven Fabrics Under Ballistic Impact," *Textile Research Journal*, Vol. 62, 1992, pp. 495–509) [using a similar fiber, Spectra® instead of Dyneema®] showed nearly a factor of 2 difference in the V_{50} velocity in the two possible stacking orders, that is, Spectra® versus Kevlar29® as the strike face. This new model extends our previous fundamental work ("A New Membrane Model for the Ballistic Impact Response and V50 Performance of Multiply Fibrous System," *International Journal of Solids and Structures*, Vol. 40, 2003, pp. 6723–6765) by addressing interference factors in terms of instantaneous material inflow to the impact cone using a convolution over current local strain around the projectile edge during its deceleration. Our previous multilayer model ("Modeling of System Effects in Ballistic Impact into Multi-Layered Fibrous Structures for Soft Body Armors," *International Journal of Fracture*, Vol. 135, 2005, pp. 219–251) ignored the interference aspect though a subsequent work ("Effects of Layer Stacking Order on the V50 Velocity of Two-Layered Hybrid Armor System," *Journal of Mechanics of Materials and Structures*, Vol. 3, 2008, pp. 627–639) approximated its effects but without instantaneous response of material inflow to local tensile strain. The current model is much more complete and produces velocity, strain, and deformation histories either to perforation or to halting the projectile. In the new model, V_{50} velocity differences with stacking order and with layer bonding versus no bonding are even larger. However, backface deflections turn out to be minimally affected. Calculations are very fast and postprocessing figures can be obtained in less than a minute using MATLAB with a laptop (2 MHz Core 2 Duo CPU 2 Gb RAM).

Nomenclature

a_0 = tensile wave speed in the material
c = transverse cone wave speed in material coordinates
$\tilde{c}$ = transverse cone wave speed in ground coordinates
E = tensile modulus of the material
h = thickness of the material
L = tensile wave front position
M_p = projectile mass
r_c = cone wave front position
r_p = radius of projectile
t = time
u = inflow displacement of the material
V = projectile velocity
V_p = projectile velocity before the impact
V_0 = projectile velocity right after the impact
V_{50} = limit velocity
γ = cone angle
Δ = transverse deflection of the material under the projectile
ε_c = strain at the cone wave front
ε_p = strain at the projectile edge
ρ = density of the material

Presented as Paper 2669 at the 50th SDM; 17th ASC; 11th NDA; 10th GSF; 5th MDO, Palm Springs CA, 4–7 May 2009; received 9 May 2009; revision received 14 July 2009; accepted for publication 14 July 2009.

*Professor, Department of Theoretical and Applied Mechanics. Member AIAA.
†Research Associate, Department of Theoretical and Applied Mechanics. Member AIAA.
‡Assistant Professor, Department of Civil Engineering.

I. Introduction

WE DEVELOP a new model to investigate the ballistic response of a hybrid, two-layered, flexible body armor system, where the individual layers are not bonded together and differ considerably in their mechanical properties. Such systems are used in body armor for public safety officers and security personnel as well as in airline cockpit doors, helicopters, and the doors of automobiles and light trucks. In one particular system consisting of an aramid (Kevlar29®) fabric and a fabric of ultrahigh molecular weight and drawn polyethylene (Dyneema® or Spectra®) it was found experimentally by Cunniff [1] that the stacking order of the two layers has a very large effect on the V_{50} limit velocity (a statistical velocity threshold for perforation obtained from several tests). It was hypothesized that placing the stiffer and lighter fibrous polyethylene layer on the strike face led to an interference effect whereby the naturally occurring impact cone of the polyethylene layer clashed with that of the Kevlar® layer. This would result in impact cone interference and a shift in load from the Kevlar29® layer to the top polyethylene layer (Dyneema® or Spectra®). The main goal of the present paper is twofold. First, we introduce a new version of the single-layer model that responds instantaneously, in terms of material inflow velocity, to the changing tension around the projectile edge as it decelerates. Second, we apply the new version to the two-layer, interfering system to study analytically the negative effects of such interference on V_{50} performance and backface deflection.

The geometry of the problem of impact into two stacked layers is shown in Fig. 1 along with several key quantities. We assume the contact between the two layers is frictionless with no bonding between them. The analysis is first performed on a unit problem assuming an initial projectile velocity $V(0) = V_0$ immediately after impact, and a constant membrane strain over time at the projectile edge, $\varepsilon_{p,i}(t) = \varepsilon_{p,0,i}$, $i = 1, 2$. This situation actually corresponds to a specific rate of projectile deceleration and profile of decreasing velocity $V(t)$, $t \geq 0$ that is artificial. However, the unit solution results can then be adapted to the more general and natural case of a projectile decelerating from membrane tension around the projectile circumference acting at cone angle $\gamma(t)$ relative to the horizontal plane of the membrane. In this case it happens that $\varepsilon_{p,i}(t)$ initially increases in time t but reaches a maximum value before decreasing to zero as the projectile stops. Note that in the analysis, V_0 is taken as the projectile velocity immediately after instantaneous momentum transfer in the contact region between the projectile and the two-layer membrane. Before contact, the projectile velocity will be a slightly larger value than V_0 depending on the ratio of the projectile mass M_p to the mass of the two-layer membrane region within the contact circle, as is easily calculated from conservation of local momentum ([2–5]).

When speaking of quantities in terms of material coordinates we mean that the quantities are with reference to the original radial location r of a material point of interest. This distinction is particularly important when discussing cone-wave velocity, whether in terms of the velocity with respect to the original position of the material particles or with respect to the current location of the material points as viewed from the ground, called ground coordinates.

For the two layers denoted, $i = 1, 2$, we define ρ_i as the material density, h_i as the thickness, and E_i as the tensile modulus of layer i, and we also have the tensile wave speeds $a_{0,i} = \sqrt{E_i/\rho_i}$. Various other quantities are involved as shown in Fig. 1, with the understanding that they all depend on time t; some also depend on r (i.e., in material coordinates). In particular, when interference exists between layers there is the common quantity $\tilde{c}$, which is the transverse cone wave speed relative to ground (i.e., in ground coordinates), but the inflow velocities of the layers $\dot{u}_i$ in material coordinates are potentially different as are the transverse cone wave speeds c_i in material coordinates. Also we let ε_i be the layer i strain in material coordinates. In addition to $\tilde{c}$, we let $\dot{u}_{c,i}$ and $\varepsilon_{c,i}$ be the inflow velocity and strain, respectively, in layer i at the position of the cone wave front, denoted $r_{c,i}$ in material coordinates. In the case of interference, the three velocities for each layer are related by

$$\tilde{c} = c_i(1 + \varepsilon_{c,i}) + \dot{u}_{c,i} \tag{1}$$

because the transverse wave is moving in stretched material, accounted for by the factor $(1 + \varepsilon_{c,i})$, and the second term accounts for the fact that the cone wave front is actually traveling in material moving toward the origin (as seen from the ground).

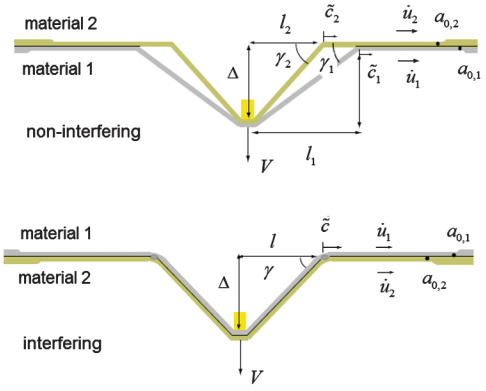

Fig. 1 Key quantities in the analysis for both the noninterfering (top) and interfering (bottom) cases.

II. Analysis for the Unit Problem Assuming Fixed Strain at the Projectile Edge

We first consider the behavior of a radially propagating tension wave in layer i, and subject to the fixed strain $\varepsilon_{p,i}(t) = \varepsilon_{p,0,i}$, $t \geq 0$, at radius $r = r_p$. This unit problem does not yet reflect the vertical deflection of the membrane by the projectile nor the change in horizontal displacement and velocity that develops at locations within the cone wave, $r_p \leq r \leq r_{c,i}(t)$, thus preventing further radial motion toward the origin. However, the associated strain profile is correct for our purposes because it is written in terms of material coordinates. Note that in the actual problem treated later, the tensile wave travels more than an order of magnitude faster than the cone wave, which in turn is similar in magnitude to the projectile velocity. Thus, near instantaneous adjustments can occur in membrane strain between the projectile radius r_p and the cone radius $r_{c,i}(t)$, as though governed by quasistatic equilibrium. Later, this will allow us to treat separately the deformation within the cone region but preserve the tension wave behavior beyond the cone wave front.

From this unit solution, the inflow displacement profile in layer $i = 1, 2$ is

$$u_i(r, t) = -\varepsilon_{p,0,i} r_p \ln\left(\frac{r_p + a_{0,i}t}{r}\right), \qquad r_p \leq r \leq r_p + a_{0,i}t \tag{2}$$

the strain profile is

$$\varepsilon_i(r, t) = \frac{\partial u_i(r, t)}{\partial r} = \varepsilon_{p,0,i}\left(\frac{r_p}{r}\right), \qquad r_p \leq r \leq r_p + a_{0,i}t \tag{3}$$

and the inflow velocity profile is

$$\dot{u}_i(r, t) = \frac{\partial u_i(r, t)}{\partial t} = -a_{0,i}\varepsilon_{p,0,i}\frac{r_p}{r_p + a_{0,i}t} \qquad r_p \leq r \leq r_p + a_{0,i}t \tag{4}$$

which we note is actually independent of radial position r. Outside this region these quantities are zero. At the projectile edge $r = r_p$, the previous relations yield

$$u_{p,i}(t) = -\varepsilon_{p,0,i} r_p \ln\left(1 + \frac{a_{0,i}t}{r_p}\right) \tag{5}$$

$$\varepsilon_{p,i}(t) = \varepsilon_{p,0,i} \tag{6}$$

and

$$\dot{u}_{p,i}(t) = -a_{0,i}\varepsilon_{p,0,i}\frac{r_p}{r_p + a_{0,i}t} \tag{7}$$

respectively, and at the cone wave front $r = r_{c,i}(t)$, these relations yield

$$u_{c,i}(t) = -\varepsilon_{p,0,i} r_p \ln\left(\frac{r_p + a_{0,i}t}{r_{c,i}(t)}\right) \tag{8}$$

$$\varepsilon_{c,i}(t) = \varepsilon_{p,0,i}\frac{r_p}{r_{c,i}(t)} \tag{9}$$

and

$$\dot{u}_{c,i}(t) = -a_{0,i}\varepsilon_{p,0,i}\frac{r_p}{r_p + a_{0,i}t} \tag{10}$$

where again we note the independence with respect to $r_{c,i}(t)$.

A. Change in Radial Length Compatibility

As is discussed later, in the formation of the cone wave representing the vertical deflection of the membrane by the projectile, a key requirement in the interfering layers is compatibility in the change in length from the tensile wave fronts at $L_i(t) = r_p + a_{0,i}t$ back to the projectile impact circle of radius r_p, because beyond that wave front the material is undisturbed, and inside both materials

follow the same geometric path to the projectile edge. For layer i, the change in length due to the strain distribution of the tension wave is defined as $\Delta l_i(t)$, and from Eq. (3) we obtain

$$\Delta l_i(t) = \int_{r_p}^{r_p + a_{0,i}t} \varepsilon_i(r,t)\,\mathrm{d}r = \varepsilon_{p,0,i} r_p \int_{r_p}^{r_p + a_{0,i}t} \frac{1}{r}\,\mathrm{d}r$$
$$= \varepsilon_{p,0,i} r_p\, \ell_n\left(\frac{r_p + a_{0,i}t}{r_p}\right) \tag{11}$$

For change-in-length compatibility we must have

$$\Delta l_1(t) = \Delta l_2(t) \equiv \Delta l(t) \tag{12}$$

so that

$$\Delta l(t) = \varepsilon_{p,0,i} r_p\, \ell_n\left(1 + \frac{t}{t_{p,i}}\right), \qquad i = 1,2 \tag{13}$$

where

$$t_{p,1} = r_p/a_{0,1}, \qquad t_{p,2} = r_p/a_{0,2} \tag{14}$$

Equations (5–14) collapse to those for the corresponding 1-D case provided that the tension wave has traveled only a small distance compared with the projectile radius, that is, $L_i(t) = r_p + a_{0,i}t$ for $0 < a_{0,i}t \ll r_p$ is only slightly larger than r_p. From a Taylor series expansion of the logarithm in Eq. (13), that is, $\ell_n(1+z) = z - z^2/2 + z^3/3 - \cdots$, we find that

$$\varepsilon_{p,1} a_{0,1} \approx \varepsilon_{p,2} a_{0,2}, \qquad 0 \le t \ll t_{p,1} \quad \text{and} \quad 0 \le t \ll t_{p,2} \tag{15}$$

or

$$\frac{\varepsilon_{p,1}}{\varepsilon_{p,2}} \to \frac{\varepsilon_{p,0,1}}{\varepsilon_{p,0,2}} = \frac{a_{0,2}}{a_{0,1}} \quad \text{as } t \to 0 \tag{16}$$

However, for longer times, where the tension wave has traveled a large distance, that is, $r_p \ll L_i(t) = r_p + a_{0,i}t$, we approximately have

$$\varepsilon_{p,1}\, \ell_n\left(\frac{t}{t_{p,1}}\right) \approx \varepsilon_{p,2}\, \ell_n\left(\frac{t}{t_{p,2}}\right), \qquad t_{p,1} \ll t \quad \text{and} \quad t_{p,2} \ll t \tag{17}$$

It can be seen immediately that to satisfy the change-in-length compatibility condition the strains at the projectile edge cannot simultaneously satisfy both Eqs. (16) and (17), and thus, must be allowed to adjust with time, which is fundamentally different from what occurs in the 1-D model of a two-layer tape. However, as will be shown later, it turns out that an effective set of strains and velocities can be defined such that the two-layer system can be treated as a single-layer unit problem, where the effective strain at the projectile edge is fixed in time. Thus, we allow the individual layer strains at the projectile edge to moderately adjust over time, and we use the notation $\varepsilon_{p,i}(t)$, $i = 1, 2$ to reflect this adjustment. Thus by Eq. (17), change-in-length compatibility means we must have

$$\frac{\varepsilon_{p,1}(t)}{\varepsilon_{p,2}(t)} = \frac{\ell_n(t/r_{p,1})}{\ell_n(t/t_{p,2})} = \frac{\ell_n(t) - \ell_n(t_{p,1})}{\ell_n(t) - \ell_n(t_{p,2})} \to 1 \quad \text{as } t \to \infty \tag{18}$$

so that the ratio of the two strains must eventually approach unity, rather than the ratio of tensile wave speeds, reflected in Eq. (16). Fortunately, the strain convolution of unit solutions performed later permits automatically handling of such strain differences between layers.

For the inflow velocity, and again ignoring the lateral deflection effects forming the cone wave, we have Eqs. (4), (7), and (10). Again, using a Taylor series expansion in the time period after impact at the cone wave front we have

$$\dot{u}_{c,i}(t) = -a_{0,i}\varepsilon_{p,0,i}\frac{1}{1 + t/t_{p,i}} = -a_{0,i}\varepsilon_{p,0,i}\left(1 - \left(\frac{t}{t_{p,i}}\right) + \left(\frac{t}{t_{p,i}}\right)^2 - \left(\frac{t}{t_{p,i}}\right)^3 + \cdots\right), \qquad i = 1,2 \tag{19}$$

Thus, for short times we see from Eq. (19) that the two inflow velocities are the same, that is,

$$\dot{u}_{c,1}(t) \approx \dot{u}_{c,2}(t) \approx -a_{0,1}\varepsilon_{p,0,1}$$
$$0 < t \ll t_{p,1} \quad \text{and} \quad 0 < t \ll t_{p,1} \tag{20}$$

or

$$\frac{\dot{u}_{c,1}(t)}{\dot{u}_{c,2}(t)} \to 1 \quad \text{as } t \to 0 \tag{21}$$

However, for much longer times we see that

$$\dot{u}_{c,i}(t) = -a_{0,i}\varepsilon_{p,0,i}\frac{1}{1 + t/t_{p,i}} \approx -\frac{a_{0,i}\varepsilon_{p,0,i}t_{p,i}}{t}$$
$$= -\frac{\varepsilon_{p,0,i}r_p}{t}, \qquad t_{p,i} \ll t \quad \text{and} \quad i = 1,2 \tag{22}$$

so that both decay rapidly to zero in inverse proportion to time t. We see, however, that Eqs. (21) and (22) cannot be satisfied simultaneously, and that the inflow velocity ratio tends to follow the ratio of the strains. However, as we have just seen, the strain at the projectile edge must adjust itself as time progresses so that the strain ratio eventually satisfies Eq. (19). Thus replacing $\varepsilon_{p,0,i}$ in Eq. (22) with $\varepsilon_{p,i}(t)$ again results in

$$\frac{\dot{u}_{c,1}(t)}{\dot{u}_{c,2}(t)} \approx \frac{\varepsilon_{p,1}(t)}{\varepsilon_{p,2}(t)} \to 1, \quad \text{as } t \to \infty \tag{23}$$

The two results, Eqs. (21) and (23), suggest that the inflow velocities will remain approximately the same over time at the cone wave front (and within the cone region), though by Eq. (22) both velocities rapidly decay to zero so that the absolute difference quickly vanishes. This equivalence can also be argued from the perspective that the inflow displacements, $u_{p,i}(t)$, at $r = r_p$ and given by Eq. (6), are the same for all time, because they are the same as $\Delta l(t)$ given by Eq. (14). However, in general (and without considering lateral deflection to form the cone) there is very little difference between the inflow velocities evaluated at $r = r_p$ and those evaluated at $r = r_{c,i}(t)$ in this two-layer version of the unit problem, and in the single-layer unit problems, Eq. (8) compared with Eq. (11) shows there is no difference at all.

B. Further Evaluation of the Strain Balance at the Projectile Edge

As was already noted, an important consequence of interference is that it is not possible for a projectile velocity profile $V(t)$, $t \ge 0$ to be chosen that yields unit solutions for each layer preserving both length compatibility and the same strain at the projectile edge for all times. Thus the unit solution viewpoint requires modifications to accommodate such changes over time, however modest. There are two main regimes of time: 1) a short time regime corresponding to unequal layer strains and growth of the tension wave up to about one projectile diameter and compatible with the 1-D solution, and 2) a much longer time regime, where the layer strains approach equality when the tension wave front has grown to become large compared with the projectile radius.

Although this second regime eventually dominates behavior in the unit problem, the first regime determines initial values. In the actual problem, the question arises as to whether the first regime can dominate behavior at times much larger than $t_{p,i}$ and even larger than suggested by the unit problem results. This is potentially an issue because, in the actual problem, the strains $\varepsilon_{p,i}(t)$ initially increase quite rapidly until they reach a peak value at times much larger than $t_{p,i}$, and the solution of the actual problem is structured as a Duhamel

convolution integral of time-delayed unit solutions of magnitude $d\varepsilon_{p,i}(t)$ after the initial step to $\varepsilon_{p,0,i}$ right after impact. Thus, the first regime could conceivably influence behavior until the peak strain has been reached, after which all quantities decay to zero as the projectile stops.

This potential influence has been investigated by studying length changes associated with impact into a single membrane layer where the correct calculation for length change over time in the actual problem would be a convolution on Eq. (14) with respect to changing strain in time, giving

$$\Delta l(t) = \Delta l_{\text{unit}}(t) + \int_0^t \frac{\dot{\varepsilon}_p(s)}{\varepsilon_{p,0}} \Delta l_{\text{unit}}(t-s)\,\mathrm{d}s \tag{24}$$

where $\Delta l_{\text{unit}}(t)$ is the unit solution change in length given by Eq. (13). Direct substitution thus gives

$$\Delta l(t) = r_p \varepsilon_{p,0}\, \ell_n\left(1+\frac{t}{t_p}\right) + r_p \int_0^t \dot{\varepsilon}_p(s)\, \ell_n\left(1+\frac{t-s}{t_p}\right)\mathrm{d}s \tag{25}$$

On the other hand, a simplified calculation of direct substitution of strain $\varepsilon_p(t)$ for $\varepsilon_{p,0}$ into $\Delta l_{\text{unit}}(t)$ yields

$$\tilde{\Delta} l(t) = \frac{\varepsilon_p(t)}{\varepsilon_{p,0}} \Delta l_{\text{unit}}(t) = \varepsilon_p(t) r_p\, \ell_n\left(1+\frac{t}{t_p}\right) \tag{26}$$

Figure 2 shows the evolving shifts in the strain ratio from the initial ratio $a_{0,1}/a_{0,2} = 1.5$ down to 1.0 at long dimensionless times (normalized in terms of the layer with the fastest tensile wave speed). The solid line is the calculated value from using the convolution and the dotted line is a simplified representation of the ratio of the strains anticipated in each layer as given by

$$\frac{\varepsilon_{p,2}(t)}{\varepsilon_{p,1}(t)} = \frac{\ell_n(1+t/t_{p,1})}{\ell_n(1+t/t_{p,2})} \tag{27}$$

where at the extremes in time we have

$$\frac{\varepsilon_{p,2}(t)}{\varepsilon_{p,1}(t)} \approx \begin{cases} a_{0,1}/a_{0,2}, & 0 \le t \ll t_{p,i} \\ 1, & t_{p,i} \ll t \end{cases} \tag{28}$$

Two cases are considered in Fig. 2, a very high fabric to projectile areal density ratio and a low fabric to projectile areal density ratio. The ratio $R_{\Delta l}(t) = \tilde{\Delta} l(t)/\Delta l(t)$ was found to be fairly close to unity over the range from impact to well past the point where the maximum strain occurs. This same behavior is seen for the full range of practical membrane to projectile areal density ratios. This indicates that, as the strain builds up to the point of maximum strain, the delay effect in the convolution is small and only very late in the slowing of the projectile is an effect modestly noticeable. In any event the progressive shift in strain ratio is important to the overall response and cannot be ignored.

The convolution formulation used to treat the problem is capable of accommodating arbitrarily differing strain histories and ratios in the individual layers. However, the analysis is greatly simplified using Eq. (27) because we will be able to define effective parameters such that the problem reduces to treatment of an effective single layer from which individual strain histories and other quantities can be calculated subsequently. One interesting feature is that the effective tensile wave speed, which we denote as $\hat{a}_0(t)$, will actually change slightly over time.

C. Pulley Analogy for Cone Wave Speed Determination

To explicitly determine the various model strains, displacements, and velocities we must specifically determine how the cone wave velocity depends on the individual layer strains $\varepsilon_{c,i}(t)$, $i = 1, 2$, at the cone wave front. The calculation is an instantaneous calculation in strain, so it applies to the case of time-dependent strain variation at the projectile edge and cone wave front. We consider the tensions and linear densities in layers 1 and 2 and the material forces that occur as the cone wave front passes by and the material suddenly changes velocity direction from horizontal inflow to nearly vertical motion at the same speed as the projectile. For this purpose we use the analogy of two thin belts, of thickness h_1 and h_2, traveling at constant velocity over a small pulley of radius $\hat{r}$, and with one on top of the other such that there is a contact pressure between the two as they pass around the pulley, thus mimicking the interference. We then determine a critical velocity such that the contact pressure between the innermost belt (the lower layer) and the small pulley itself actually shrinks to zero (because the pulley is virtual and does not actually exist to support load). This critical velocity, corresponding to $c_i(t)[1+\varepsilon_{c,i}(t)]$ in the stretched material, is the critical speed of the material passing over the pulley to yield a vanishing contact force with the pulley. Furthermore, we will find that the critical velocity is independent of the pulley radius $\hat{r}$, and so is the total interactive force at the cone wave front acting along a line bisecting the wraparound angle $\alpha(t) = \pi - \gamma(t)$.

A simple geometric analysis of the centrifugal forces acting over a small wraparound angle increment $d\alpha$shows that the contact force per unit length N_i for layer i is

$$N_i \hat{r}\,\mathrm{d}\alpha = 2F_i \frac{\mathrm{d}\alpha}{2} - \frac{\{\rho_i h_i/[1+\varepsilon_{c,i}(t)]\}\{c_i(t)[1+\varepsilon_{c,i}(t)]\}^2 \hat{r}\,\mathrm{d}\alpha}{\hat{r}} \tag{29}$$

where we have accounted for the slight drop in mass per unit length due to the stretching of the material. Because

$$F_i(t) = h_i E_i \varepsilon_{c,i}(t), \qquad i = 1, 2 \tag{30}$$

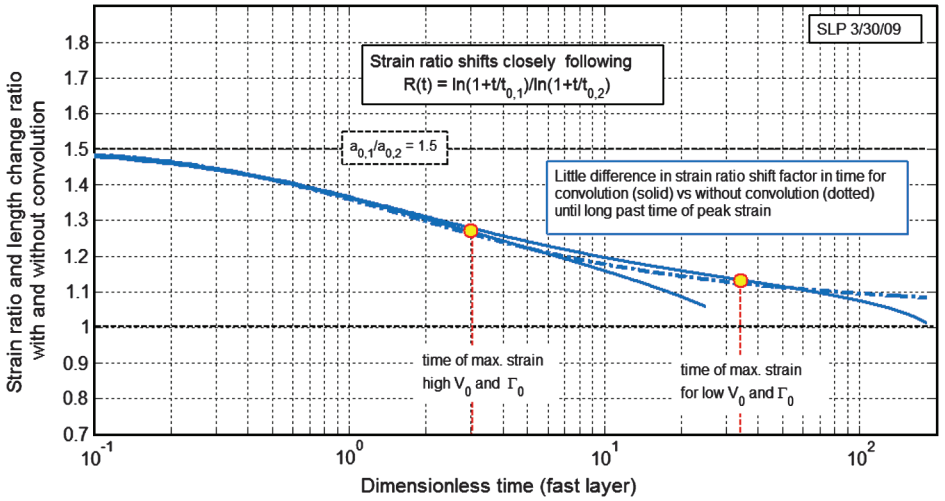

Fig. 2 Assessment of changes of the ratio of strains in the two layers over time.

we have

$$N_i(t)\ddot{r} = h_i E_i \varepsilon_{c,i}(t) - \rho_i h_i c_i^2(t)[1+\varepsilon_{c,i}(t)], \qquad i=1,2 \quad (31)$$

To have vanishing contact pressure onto the pulley (which does not exist in the actual problem) we must have

$$N_1(t)\ddot{r} + N_2(t)\ddot{r} = 0 \quad (32)$$

Substituting Eq. (31) into Eq. (32) results in

$$h_1 E_1 \varepsilon_{c,1}(t) + h_2 E_2 \varepsilon_{c,2}(t) = \frac{\rho_1 h_1 \{c_1(t)[1+\varepsilon_{c,1}(t)]\}^2}{1+\varepsilon_{c,1}(t)} + \frac{\rho_2 h_2 \{c_2(t)(1+\varepsilon_{c,2}(t)]\}^2}{1+\varepsilon_{c,2}(t)} \quad (33)$$

Because $a_{0,i}^2 = E_i/\rho_i$ we can rewrite Eq. (33) as

$$\rho_1 h_1 [1+\varepsilon_{c,1}(t)]c_1^2(t) + \rho_2 h_2 [1+\varepsilon_{c,2}(t)]c_2^2(t) = \rho_1 h_1 a_{0,1}^2 \varepsilon_{c,1}(t) + \rho_2 h_2 a_{0,2}^2 \varepsilon_{c,2}(t) \quad (34)$$

and because $c_1(t)[1+\varepsilon_{c,1}(t)] \approx c_2(t)[1+\varepsilon_{c,2}(t)]$ we have

$$\{c_i(t)[1+\varepsilon_{c,i}(t)]\}^2 = \frac{\rho_1 h_1 a_{0,1}^2 \varepsilon_{c,1}(t) + \rho_2 h_2 a_{0,2}^2 \varepsilon_{c,2}(t)}{\rho_1 h_1/[1+\varepsilon_{c,1}(t)] + \rho_2 h_2/[1+\varepsilon_{c,2}(t)]} \quad (35)$$

D. Cone Wave Speed Behavior Immediately After Impact

Right after impact, when $0 < a_{0,i}t \ll r_p$ we have Eq. (16) or $\varepsilon_{p,0,1}a_{0,1} \approx \varepsilon_{p,0,2}a_{0,2}$ and can assume $r_{c,0,i} \approx r_p$. We apply subscript 0 to signify quantities immediately after impact, and have $\varepsilon_{c,0,i} \approx \varepsilon_{p,0,i}$ by Eq. (10), in which case $\varepsilon_{c,0,1}a_{0,1} \approx \varepsilon_{c,0,2}a_{0,2}$. Also

$$c_{0,1}(1+\varepsilon_{c,0,1}) = c_{0,2}(1+\varepsilon_{c,0,2}) = \tilde{c}_0 - \dot{u}_{c,0,2} = \tilde{c}_0 - \dot{u}_{c,0}$$
$$\dot{u}_{c,0} = -a_{0,1}\varepsilon_{p,0,1} \quad (36)$$

where equality reflects the limit as $t \to 0$. Thus, Eq. (35) becomes

$$[c_{0,i}(1+\varepsilon_{p,0,i})]^2 = a_{0,i}\varepsilon_{p,0,i}\left[\frac{a_{0,1}\rho_1 h_1 + a_{0,2}\rho_2 h_2}{\rho_1 h_1/(1+\varepsilon_{p,0,1}) + \rho_2 h_2/(1+\varepsilon_{p,0,2})}\right] \quad (37)$$

This situation has been investigated in the case of a two-layer tape system in one dimension, where it has been found that an effective set of parameters can be introduced, as described in Appendix A. The effective parameters $\hat{c}_0$, $\hat{\varepsilon}_{p0}$, and $\hat{a}_{00}$ are given by

$$\hat{c}_0(1+\hat{\varepsilon}_{p0}) = c_{0,1}(1+\varepsilon_{p,0,1}) = c_{0,2}(1+\varepsilon_{p,0,2}) \quad (38)$$

$$\hat{a}_{00} = \frac{a_{0,1}\rho_1 h_1/(1+\varepsilon_{p,0,1}) + a_{0,2}\rho_2 h_2/(1+\varepsilon_{p,0,2})}{\rho_1 h_1/(1+\varepsilon_{p,0,1}) + \rho_2 h_2/(1+\varepsilon_{p,0,2})} \quad (39)$$

which is accurately approximated by

$$\hat{a}_{00} \approx \frac{a_{0,1}\rho_1 h_1 + a_{0,2}\rho_2 h_2}{\rho_1 h_1 + \rho_2 h_2} \quad (40)$$

because the neglected strains are small and not too different in value. Also

$$\hat{\varepsilon}_{p0} = \frac{a_{0,1}}{\hat{a}_{00}}\varepsilon_{p,0,1} = \frac{a_{0,2}}{\hat{a}_{00}}\varepsilon_{p,0,2} \quad (41)$$

Most important we find that Eq. (37) reduces to

$$\hat{c}_0 = \hat{a}_{00}\sqrt{\frac{\hat{\varepsilon}_{p0}}{1+\hat{\varepsilon}_{p0}}} \quad (42)$$

An additional result needed from the 1-D model is the compatibility of the flow of stretched material into the cone region with the growth of the length (hypotenuse) spanning from the cone wave front to the projectile edge. The relevant result is

$$c_{0,i}(1+\varepsilon_{p,0,i}) = \sqrt{[c_{0,i}(1+\varepsilon_{p,0,i}) - \varepsilon_{p,0,i}a_{0,i}]^2 + (V_0)^2} \quad i=1,2 \quad (43)$$

which by Eqs. (38–42) can be written in terms of the effective parameters as

$$\hat{c}_0(1+\hat{\varepsilon}_{p0}) = \sqrt{[\hat{c}_0(1+\hat{\varepsilon}_{p0}) - \hat{\varepsilon}_{p0}\hat{a}_{00}]^2 + (V_0)^2} \quad (44)$$

Squaring both sides and manipulating the result leads to a quadratic that can be factored to yield

$$\hat{c}_0 = \hat{a}_{00}\left\{1 - \sqrt{1 - \left(\frac{V_0}{\hat{c}_0(1+\hat{\varepsilon}_{p0})}\right)^2}\right\}, \qquad i=1,2 \quad (45)$$

Eliminating $\hat{c}_0$ using Eq. (42) and manipulating the result gives

$$\hat{\varepsilon}_{p0} = \left[\frac{1}{4(1+\hat{\varepsilon}_{p0})}\right]^{1/3}\left[\left(\frac{V_0}{\hat{a}_{00}}\right)^2 + \hat{\varepsilon}_{p0}^2\right]^{2/3} \quad (46)$$

This is used to establish initial conditions on the effective strain $\hat{\varepsilon}_{p0}$ upon impact.

Rather than solve Eq. (46) numerically, we can develop an accurate approximation through iteration. A first approximation for the strain on impact is

$$\hat{\varepsilon}_{p0} \approx \hat{\varepsilon}_{p0}^{(1)} = \left(\frac{V_0}{\sqrt{2}\hat{a}_{00}}\right)^{4/3} \quad (47a)$$

and a second, more accurate approximation is

$$\hat{\varepsilon}_{p0} \approx \hat{\varepsilon}_{p0}^{(2)} = \left(\frac{V_0}{\sqrt{2}\hat{a}_{00}}\right)^{4/3}\left(\frac{1}{1+\hat{\varepsilon}_{p0}^{(1)}}\right)^{1/3}\left[1+\left(\frac{\hat{\varepsilon}_{p0}^{(1)}\hat{a}_{00}}{V_0}\right)^2\right]^{2/3} \quad (47b)$$

A third and extremely accurate approximation that we use is

$$\hat{\varepsilon}_{p0} \approx \hat{\varepsilon}_{p0}^{(3)} = \left(\frac{V_0}{\sqrt{2}\hat{a}_{00}}\right)^{4/3}\left(\frac{1}{1+\hat{\varepsilon}_{p0}^{(2)}}\right)^{1/3}\left[1+\left(\frac{\hat{\varepsilon}_{p0}^{(2)}\hat{a}_{00}}{V_0}\right)^2\right]^{2/3} \quad (47c)$$

Once $\hat{\varepsilon}_{p0}$ is known, the starting strain values right after impact are simply

$$\varepsilon_{p,0,1} = \frac{\hat{a}_{00}}{a_{0,1}}\hat{\varepsilon}_{p,0}, \qquad \varepsilon_{p,0,2} = \frac{\hat{a}_{00}}{a_{0,2}}\hat{\varepsilon}_{p,0} \quad (48)$$

E. Cone Wave Speed Behavior at Longer Times after Impact

The case of longer times has been treated in Appendix B. There it is shown that an effective set of parameters $\hat{c}(t)$, $\hat{\varepsilon}_c(t)$, $\hat{\varepsilon}_p(t)$, and $\hat{a}_0(t)$ can again be defined to reduce the two-layer impact problem with interference to one of impact into a single layer. Again, individual layer strains and other quantities can be calculated from the results. The most crucial quantity is the effective tensile wave speed

$$\hat{a}_0(t) = \sqrt{\frac{\rho_1 h_1 a_{0,1}^2\left\{\frac{\ell n[1+\hat{a}_0(t)t/r_p]}{\ell n(1+a_{0,1}t/r_p)}\right\} + \rho_2 h_2 a_{0,2}^2\left\{\frac{\ell n[1+\hat{a}_0(t)t/r_p]}{\ell n(1+a_{0,2}t/r_p)}\right\}}{\rho_1 h_1 + \rho_2 h_2}} \quad (49a)$$

which unfortunately is an implicit equation $\hat{a}_0(t)$ that would require numerical solution. However, in Appendix C we show that a very accurate approximation results from using $\hat{a}_{00}$ in place of $\hat{a}_0(t)$ on the

right-hand side and furthermore, it yields the correct limits at short and long times. Specifically, this approximation is

$$\hat{a}_0(t) \approx \sqrt{\frac{\rho_1 h_1 a_{0,1}^2 \left[\frac{\ell_n(1+\hat{a}_{00}t/r_p)}{\ell_n(1+a_{0,1}t/r_p)}\right] + \rho_2 h_2 a_{0,2}^2 \left[\frac{\ell_n(1+\hat{a}_{00}t/r_p)}{\ell_n(1+a_{0,2}t/r_p)}\right]}{\rho_1 h_1 + \rho_2 h_2}} \quad (49b)$$

We also have a key result, namely

$$\hat{c}(t) = \hat{a}_0(t)\sqrt{\frac{\hat{\varepsilon}_c(t)}{1+\hat{\varepsilon}_c(t)}} \quad (50)$$

Once the effective strain $\hat{\varepsilon}_c(t)$ is found from the effective single-layer calculation, the individual strains can be found from an adaptation of Eq. (27), namely

$$\varepsilon_{c,i}(t) = \hat{\varepsilon}_c(t)\frac{\ell_n[1+\hat{a}_0(t)t/r_p]}{\ell_n(1+\hat{a}_{0,i}t/r_p)}, \qquad i=1,2 \quad (51)$$

Also, right after impact we have $\hat{a}_0(0) = \hat{a}_{00}$ from Eq. (40) and $\hat{\varepsilon}_c(0) = \hat{\varepsilon}_p(0) = \hat{\varepsilon}_{p0}$ from Eqs. (47a–47c), as well as the starting cone wave speed, $\hat{c}(0) = \hat{c}_0$ from Eq. (42).

III. Solution Approach for Varying Projectile Velocity and Local Strain

The solution approach for the case of varying projectile velocity under decelerating forces from the two-layer membrane system, and with initial velocity V_0 right after impact, can be adapted from the same problem for a single membrane layer. All that is necessary is to use the effective property parameter set $\hat{a}_0(t)$, $\hat{\varepsilon}_p(t)$, $\hat{\varepsilon}_c(t)$, and $\hat{c}(t)$, and the initial values as just described.

Key equations from the 2-D membrane analysis are given as follows. We let the displacement be

$$\Delta(t) = \int_0^t V(s)\,\mathrm{d}s \quad (52)$$

and the effective cone wave front position be

$$\hat{r}_c(t) = r_p + \int_0^t \hat{c}(\tau)\,\mathrm{d}\tau \quad (53)$$

which is the effective position of the cone wave front in material coordinates where $\hat{c}(t)$ is given by Eq. (50).

Also we denote $\hat{u}_c(t)$ as the inflow displacement at the cone wave front and $\dot{\hat{u}}_c(t)$ as the inflow velocity (toward the impact region) of the material points at the cone wave (material coordinates). Then the cone wave speed with respect to ground is

$$\tilde{c}(t) = \hat{c}(t)[1+\hat{\varepsilon}_c(t)] + \dot{\hat{u}}_c(t) \quad (54)$$

The cone angle with respect to ground is given by

$$\sin\gamma(t) = \frac{\delta(t)}{\sqrt{[\hat{r}_c(t)+\hat{u}_c(t)-r_p]^2+\delta(t)^2}} \quad \text{and}$$
$$\cos\gamma(t) = \frac{\hat{r}_c(t)+\hat{u}_c(t)-r_p}{\sqrt{[\hat{r}_c(t)+\hat{u}_c(t)-r_p]^2+\delta(t)^2}} \quad (55)$$

and from considerations of the growth rate of the cone side (hypotenuse), we have the 2-D single-layer-based result

$$\hat{c}(t)[1+\hat{\varepsilon}_c(t)] = \frac{\cos\gamma(t)\dot{\hat{u}}_c(t) + \sin\gamma(t)V(t)}{1-\cos\gamma(t)} \quad (56)$$

We also have the instantaneous behavior

$$\hat{\varepsilon}_p(t) = \hat{\varepsilon}_c(t)\frac{\hat{r}_c(t)}{r_p} \quad (57)$$

and for the cone wave front radius using the 2-D single-layer result derived in Appendix C we also have that

$$\frac{\hat{r}_c(t)}{r_p} = \left[\frac{3}{2}\frac{\hat{a}_0(t)}{r_p}\int_0^t \sqrt{\hat{\varepsilon}_p(s)}\,\mathrm{d}s + (1+\hat{\varepsilon}_{p0})^{3/2}\right]^{2/3} - \hat{\varepsilon}_{p0} \quad (58)$$

Turning to Eqs. (54–57) we can derive

$$\sqrt{\hat{\varepsilon}_c(t)[1+\hat{\varepsilon}_c(t)]} = \kappa_c(t) \quad (59)$$

where

$$\kappa_c(t) = \frac{1}{\hat{a}_0(t)}\left[\frac{\cos\gamma(t)\dot{\hat{u}}_c(t) + \sin\gamma(t)V(t)}{1-\cos\gamma(t)}\right] \quad (60)$$

Squaring Eq. (60) and factoring the quadratic in $\varepsilon_c(t)$ we obtain

$$\hat{\varepsilon}_c(t) = \frac{\sqrt{1+4\kappa_c(t)^2}-1}{2} \quad (61)$$

and by Eq. (57) we obtain

$$\hat{\varepsilon}_p(t) = \left[\frac{\hat{r}_c(t)}{2r_p}\right][\sqrt{1+4\kappa_c(t)^2}-1] \quad (62)$$

Considering now the inflow displacement $\hat{u}_c(t)$ and velocity $\dot{\hat{u}}_c(t)$, we use the unit solutions developed earlier in a Duhamel convolution integral. From Eq. (8) we obtain

$$\hat{u}_c(t) = -\hat{\varepsilon}_{p0} r_p\,\ell_n\left[\frac{r_p+\hat{a}_0(t)t}{\hat{r}_c(t)}\right] - r_p\int_0^t \frac{\mathrm{d}\hat{\varepsilon}_p(s)}{\mathrm{d}s}\ell_n\left[\frac{r_p+\hat{a}_0(t-s)(t-s)}{\hat{r}_c(t)}\right]\mathrm{d}s \quad (63)$$

and from Eq. (10)

$$\dot{\hat{u}}_c(t) = -\frac{\hat{a}_0(t)\hat{\varepsilon}_{p0}}{1+\hat{a}_0(t)t/r_p} - \int_0^t \frac{\mathrm{d}\hat{\varepsilon}_p(s)}{\mathrm{d}s}\frac{\hat{a}_0(t-s)}{1+\hat{a}_0(t-s)(t-s)/r_p}\,\mathrm{d}s \quad (64)$$

where in Eq. (63), the position of evaluation is the current cone wave front $\hat{r}_c(t)$, irrespective of the strain history. Thus, both $\hat{u}_c(t)$ and $\dot{\hat{u}}_c(t)$ depend on the strain history $\mathrm{d}\hat{\varepsilon}_p(s)/\,\mathrm{d}s$, $0 \le s \le t$.

To calculate the deceleration profile of the projectile, $\mathrm{d}V(t)/\,\mathrm{d}t$, we must consider the resisting force applied by the fabric and the key relation is

$$F_{\text{membrane}} = -2\pi r_p[E_1 h_1 \varepsilon_{p,1}(t) + E_2 h_2 \varepsilon_{p,2}(t)]\sin\gamma(t) = [M_p + \pi r_p^2(\rho_1 h_1 + \rho_2 h_2)]\frac{\mathrm{d}V(t)}{\mathrm{d}t}, \qquad t \ge 0 \quad (65)$$

Letting

$$\Theta_{p,i} = \frac{2\pi r_p E_i h_i}{M_p + \pi r_p^2(\rho_1 h_1 + \rho_2 h_2)}\left(\frac{r_p}{a_{0,i}^2}\right) = \frac{2\pi r_p^2 \rho_i h_i}{M_p + \pi r_p^2(\rho_1 h_1 + \rho_2 h_2)}, \qquad i=1,2 \quad (66)$$

we write Eq. (66) as

$$\frac{\mathrm{d}V(t)}{\mathrm{d}t} = -\left[\Theta_{p,1}\frac{a_{0,1}^2}{r_p}\varepsilon_{p,1}(t) + \Theta_{p,2}\frac{a_{0,2}^2}{r_p}\varepsilon_{p,2}(t)\right]\sin\gamma(t) \quad (67)$$

where the initial condition is $V(0) = V_0$. However by Eqs. (9), (51), and (57) and the fact $r_{c,1}(t) \approx r_{c,2}(t)$ we have

$$\varepsilon_{p,i}(t) = \hat{\varepsilon}_p(t)\frac{\ell_n(1+\hat{a}_0(t)t/r_p)}{\ell_n(1+a_{0,i}t/r_p)}, \qquad i=1,2 \quad (68)$$

so that

$$\frac{\mathrm{d}V(t)}{\mathrm{d}t} = -\left\{\Theta_{p,1}\frac{a_{0,1}^2}{r_p}\frac{\ell_n[1+\hat{a}_0(t)t/r_p]}{\ell_n(1+a_{0,1}t/r_p)} + \Theta_{p,2}\frac{a_{0,2}^2}{r_p}\frac{\ell_n[1+\hat{a}_0(t)t/r_p]}{\ell_n(1+a_{0,2}t/r_p)}\right\}\hat{\varepsilon}_p(t)\sin\gamma(t) \tag{69}$$

However, using Eqs. (49) and (66) we can rewrite a key quantity in Eq. (69) as

$$\begin{aligned}&\Theta_{p,1}\frac{a_{0,1}^2}{r_p}\frac{\ell_n[1+\hat{a}_0(t)t/r_p]}{\ell_n(1+a_{0,1}t/r_p)} + \Theta_{p,2}\frac{a_{0,2}^2}{r_p}\frac{\ell_n[1+\hat{a}_0(t)t/r_p]}{\ell_n(1+a_{0,2}t/r_p)}\\ &= \frac{2\pi r_p a_{0,1}^2\rho_i h_i}{M_p+\pi r_p^2(\rho_1 h_1+\rho_2 h_2)}\frac{\ell_n[1+\hat{a}_0(t)t/r_p]}{\ell_n(1+a_{0,1}t/r_p)}\\ &\quad + \frac{2\pi r_p a_{0,2}^2\rho_i h_i}{M_p+\pi r_p^2(\rho_1 h_1+\rho_2 h_2)}\frac{\ell_n[1+\hat{a}_0(t)t/r_p]}{\ell_n(1+a_{0,2}t/r_p)}\\ &= \frac{2\pi r_p\hat{a}_0^2(t)(\rho_1 h_1+\rho_1 h_1)}{M_p+\pi r_p^2(\rho_1 h_1+\rho_2 h_2)}\end{aligned} \tag{70}$$

Thus, we let

$$\hat{\Theta}_p(t) = \left(\frac{r_p}{\hat{a}_{00}^2}\right)\frac{2\pi r_p\hat{a}_0^2(t)(\rho_1 h_1+\rho_2 h_2)}{M_p+\pi r^2} \tag{71}$$

and the key differential equation reduces to

$$\frac{\mathrm{d}V(t)}{\mathrm{d}t} = -\frac{\hat{a}_{00}^2}{r_p}\hat{\Theta}_p(t)\hat{\varepsilon}_p(t)\sin\gamma(t) \tag{72}$$

with the initial condition $V(0)=V_0$. Integrating Eq. (72) we obtain

$$V(t) = V_0 - \frac{\hat{a}_{00}^2}{r_p}\int_0^t \hat{\Theta}_p(t)\hat{\varepsilon}_p(s)\sin\gamma(s)\,\mathrm{d}s \tag{73}$$

A numerical solution can be developed incrementally in small time steps as was done for the single 2-D membrane problem. The initial values are given by Eqs. (40), (42), and (47a–47c) as well as

$$\begin{aligned}&V(0)=V_0, \qquad \delta(0)=0\\ &\dot{\hat{u}}_c(0) = -\hat{a}_{00}\hat{\varepsilon}_{p0} = -a_{0,1}\varepsilon_{p,0,1} \quad \text{and} \quad \hat{u}_c(0)=0\end{aligned} \tag{74}$$

and

$$\cos\gamma(0) = \frac{\tilde{c}_0}{\sqrt{\tilde{c}_0^2+V_0^2}}, \qquad \sin\gamma(0) = \frac{V_0}{\sqrt{\tilde{c}_0^2+V_0^2}} \tag{75}$$

where

$$\tilde{c}_0 = \hat{a}_{00}\left(\sqrt{\hat{\varepsilon}_{p0}(1+\hat{\varepsilon}_{p0})}-\hat{\varepsilon}_{p0}\right) \tag{76}$$

For the case of noninterfering behavior (obtained by reversing the two-layer stacking), the layers can be treated separately. In the previous equations, a single layer is retrieved simply by making the thickness h_i of the other layer zero. The key condition governing coupling is that the reaction forces from each layer must sum to give the common deceleration $\mathrm{d}V(t)/\mathrm{d}t$, that is

$$\begin{aligned}[M_p+\pi r_p^2(\rho_1 h_1+\rho_2 h_2)]\frac{\mathrm{d}V(t)}{\mathrm{d}t} &= -2\pi r_p[E_1 h_1\varepsilon_{p,1}(t)\sin\gamma_1(t)\\ &\quad + E_2 h_2\varepsilon_{p,2}(t)\sin\gamma_2(t)], \qquad t\ge 0\end{aligned} \tag{77}$$

Letting

$$\Theta_{p,} = \frac{2\pi r_p^2\rho_i h_i}{M_p+\pi r_p^2(\rho_1 h_1+\rho_2 h_2)}\left(\frac{a_{0,i}^2}{\hat{a}_{00}^2}\right), \qquad i=1,2 \tag{78}$$

where

$$\hat{a}_{00} = \frac{a_{0,1}\rho_1 h_1 + a_{0,2}\rho_2 h_2}{\rho_1 h_1+\rho_2 h_2} \tag{79}$$

we write Eq. (77) as

$$\frac{\mathrm{d}V(t)}{\mathrm{d}t} = -\frac{\hat{a}_{00}^2}{r_p}[\Theta_{p,1}\varepsilon_{p,1}(t)\sin\gamma_1(t) + \Theta_{p,2}\varepsilon_{p,2}(t)\sin\gamma_2(t)] \tag{80}$$

with the initial condition $V(0)=V_0$. Integration gives

$$V(t) = V_0 - \frac{\hat{a}_{00}^2}{r_p}\left\{\int_0^t[\Theta_{p,1}\varepsilon_{p,1}(s)\sin\gamma_1(s) + \Theta_{p,2}\varepsilon_{p,2}(s)\sin\gamma_2(s)]\,\mathrm{d}s\right\} \tag{81}$$

For the case when the layers are bonded together one may treat the system as a one-layer system using effective properties given by

$$\begin{aligned}E_{\text{eff}} &= \frac{E_1 h_1+E_2 h_2}{h_1+h_2}, \qquad \rho_{\text{eff}} = \frac{\rho_1 h_1+\rho_2 h_2}{h_1+h_2}\\ h_{\text{eff}} &= h_1+h_2, \qquad a_{0,\text{eff}} = \sqrt{\frac{E_{\text{eff}}}{\rho_{\text{eff}}}}\end{aligned} \tag{82}$$

The strains are the same in both layers, that is, $\varepsilon_{p,1}(t)=\varepsilon_{p,2}(t)$ and $\varepsilon_{c,1}(t)=\varepsilon_{c,2}(t)$, and the failure strain is the smallest of the individual strains unless the other layer can support the total tension once the weakest layer fails.

IV. Dimensionless Framework for Numerical Solution

It is convenient to reframe the problem in terms of various dimensionless quantities to make the calculations more transparent. We let τ be dimensionless time defined by

$$\tau = t/\hat{t}_p, \qquad \hat{t}_p = r_p/\hat{a}_{00} \tag{83}$$

where $\hat{t}_p$ is the time required for the effective tensile wave front to travel a distance equal to the projectile radius, using the initial effective tensile wave-speed value $\hat{a}_{00}$ defined by Eq. (40). (Using $\hat{a}_{00}$ in the normalization provides a convenient scaling for all the results.) For the cone wave front, the normalized velocity and displacement are, respectively

$$C(\tau) = \frac{\hat{c}(\tau\hat{t}_p)}{\hat{a}_{00}} \tag{84}$$

and

$$R_c(\tau) = \frac{\hat{r}_c(\tau\hat{t}_p)}{r_p} = \frac{r_p}{r_p} + \frac{\hat{a}_{00}}{r_p}\int_0^{\tau\hat{t}_p}\frac{\hat{c}(s)}{\hat{a}_{00}}\,\mathrm{d}s = 1+\int_0^\tau C(\zeta)\,\mathrm{d}\zeta \tag{85}$$

Normalized quantities describing the various strains and strain rate are

$$\begin{aligned}&\Xi_c(\tau) \equiv \hat{\varepsilon}_c(\tau\hat{t}_p)\\ &\Xi_p(\tau) \equiv \hat{\varepsilon}_p(\tau\hat{t}_p) = \Xi_c(\tau)R_c(\tau) \quad \text{and} \quad \Xi_{p,0} = \hat{\varepsilon}_{p0}\end{aligned} \tag{86}$$

and

$$\dot{\Xi}_p(\tau) = \frac{\partial\Xi_p(\tau)}{\partial\tau} = \dot{\hat{\varepsilon}}_p(\tau)\hat{t}_p \tag{87}$$

Normalized quantities for the projectile velocity and displacement are

$$\Psi(\tau) = \frac{V(\hat{t}_p\tau)}{\hat{a}_{00}}, \qquad \Psi_0 = \frac{V_0}{\hat{a}_{00}} \tag{88}$$

and

$$\Delta(\tau) = \frac{\delta(\tau \hat{t}_p)}{r_p} = \int_0^\tau \Psi(\zeta)\, \mathrm{d}\zeta \tag{89}$$

Normalized quantities for the inflow displacement and velocity are

$$U_c(\tau) = \frac{\hat{u}_c(\hat{t}_p \tau)}{\hat{\varepsilon}_{p0} r_p}$$

$$\dot{U}_c(\tau) = \frac{\partial U_c(\tau)}{\partial \tau}, \quad \text{and} \quad \dot{U}_{c,0} = \frac{\dot{\hat{u}}_c(0)}{\hat{\varepsilon}_{p0} \hat{a}_{00}} = -1 \tag{90}$$

Normalizing the cone wave speed in ground coordinates, Eq. (50) with Eq. (57) becomes

$$C(\tau) = A(\tau)\sqrt{\frac{\Xi_c(\tau)}{1+\Xi_c(\tau)}} = A(\tau)\sqrt{\frac{\Xi_p(\tau)}{R_c(\tau)+\Xi_p(\tau)}} \tag{91a}$$

where

$$\mathrm{A}\,(\tau) = \frac{\hat{a}_0(\hat{t}_p \tau)}{\hat{a}_{00}} \tag{91b}$$

directly reflects the mildly changing effective tensile wave speed over time. Also Eq. (58) becomes

$$R_c(\tau) = \left[\frac{3A(\tau)}{2}\int_0^\tau \sqrt{\Xi_p(\zeta)}\, \mathrm{d}\zeta + (1+\Xi_{p,0})^{3/2}\right] - \Xi_{p,0} \tag{92}$$

The cone angle is reparameterized as $\Gamma(\tau) = \gamma(\hat{t}_p \tau)$ so that

$$\sin\Gamma(\tau) = \sqrt{1-\cos^2\Gamma(\tau)} = \frac{\Delta(\tau)}{\sqrt{[R_c(\tau)+\Xi_{p,0}U_c(\tau)-1]^2+\Delta(\tau)^2}} \tag{93}$$

Also from Eqs. (59–62) we have

$$\Xi_p(\tau) = \frac{R_c(\tau)}{2}[\sqrt{1+4K_c(\tau)^2}-1] \tag{94}$$

where

$$K_c(\tau) \equiv \kappa_c(\hat{t}_p \tau) = \frac{\cos\Gamma(\tau)\Xi_{p,0}\dot{U}_c(\tau) + \sin\Gamma(\tau)\Psi(\tau)}{A(\tau)[1-\cos\Gamma(\tau)]} \tag{95}$$

Furthermore Eq. (72) becomes

$$\frac{\mathrm{d}\Psi(\tau)}{\mathrm{d}\tau} = -\hat{\Theta}_p \Xi_p(\tau)\sin\Gamma(\tau)$$

$$\hat{\Theta}_p(t_p\tau) = A^2(\tau)\frac{2\pi r_p^2(\rho_1 h_1 + \rho_2 h_2)}{M_p + \pi r_p^2(\rho_1 h_1 + \rho_2 h_2)} \tag{96}$$

For the initial conditions we can iteratively solve

$$\Xi_{p,0} = \left(\frac{\Psi_0}{\sqrt{2}}\right)^{4/3}\left(\frac{1}{1+\Xi_{p,0}}\right)^{1/3}\left[1+\left(\frac{\Xi_{p,0}}{\Psi_0}\right)^2\right]$$

$$\Psi_0 = V_0/\hat{a}_{00} \tag{97}$$

as was done in Eqs. (47a–47c). Also

$$\Psi_0 = V_0/\hat{a}_{00}, \qquad \Delta(0) = \Delta_0 = 0$$

$$\dot{U}_c(0) = \dot{U}_{c,0} = -1 \quad \text{and} \quad U_c(0) = U_{c,0} = 0 \tag{98}$$

as well as

$$\sin\Gamma(0) = \frac{\Psi_0}{\sqrt{[\sqrt{\Xi_{p,0}/(1+\Xi_{p,0})} - \Xi_{p,0}]^2 + \Psi_0^2}}$$

$$\cos\Gamma(0) = \sqrt{1-\sin^2\Gamma(0)} \tag{99}$$

V. Application to Kevlar®/Spectra® Hybrid System

We have applied the resulting new model to hybrid multilayer problems with and without interlayer bonding and interference among plies. For this purpose we have revisited the well-known experimental study on system effects in a Kevlar29®/Spectra® hybrid system originally published by Cunniff [1] and studied in our most recent work [2]. The mechanical properties of the two materials were 1) Kevlar®: $A_{d,K} = 0.29$ Kg/m^2 (areal density), $\rho_K = 1,450$ Kg/m^3 (material density), 2) $E_{K,\mathrm{yarn}} = 79$ GPa, and 3) Spectra®: $A_{d,S} = 0.18$ Kg/m^2 (areal density), $\rho_S = 970$ Kg/m^3 (material density), $E_{S,\mathrm{yarn}} = 120$ GPa.

The projectile radius and mass were 2.76 mm and 16 grains (1.04 g), respectively. In the model the modulus for each layer is $E_i = E_{i,\mathrm{yarn}}/2$ because of the yarn crossings to form an isotropic sheet. Their tensile wave velocities are, respectively, $a_{0,K} = \sqrt{E_K/\rho_K} = 5,219$ and $a_{0,S} = \sqrt{E_S/\rho_S} = 7,865$ m/s, so that with the higher Spectra® modulus and lower density, the tensile wave speeds differ substantially. It should also be noticed that in Cunniff's study, the areal density ratio of total membrane to projectile $\Gamma_0 = 0.01084$ is an order of magnitude lower than in typical body armor, and so the maximum experimental V_{50} velocities ~200 m/s are relatively low compared with real body armor.

Cunniff [1] showed that reversing the order of Spectra® and Kevlar® layers had a large effect on the V_{50} penetration velocity, and

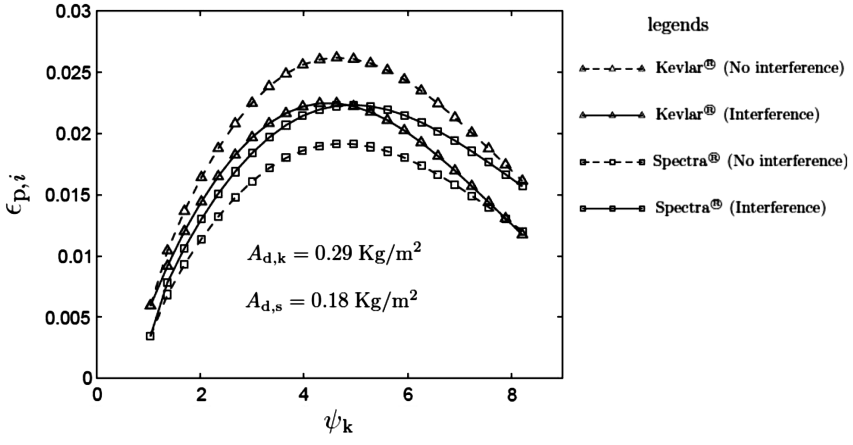

Fig. 3 Layer strain evolution predicted in Porwal and Phoenix [2] for the experimental system of Cunniff [1] (assuming Spectra® modulus of 120 GPa) showing significant differences in strain patterns depending on whether the layers are interfering or noninterfering. Impact velocity is 140 m/s.

the worst case resulted from placing the Spectra® layer first, in large part because of interference effects of the much higher tensile wave speed in the Spectra® layer compared with the Kevlar® layer and the much lower material density. The results from our previous modeling work [2], which used retroactive strain substitution, confirmed Cunniff's [1] findings. Figure 3 shows some results from that version, where ψ_K is normalized growth of the cone wave edge (normalized by the projectile radius).

As a benchmark test of the new model and code with the Duhamel convolution we reran the calculations on the Cunniff hybrid system [1]. Additionally we investigated the effect in Cunniff's system of some reported ballistic stiffening effects seen in Spectra® by Prevorsek et al. [3] and Dyneema® (private communication from manufacturer DSM) whereby the tensile modulus at ballistic loading rates is typically a much higher value, 200 GPa, rather than the 120 GPa value used by Cunniff, based on tension tests at strain rates of 0.05/ min. In this case the Spectra® tensile wave speed becomes $a_{0,S} = \sqrt{E_S/\rho_S} = 10,153$ m/s, approximately double that for the Kevlar29® layer.

Figures 4 and 5 compare various cases: 1) bonded layers, 2) noninterfering layers (i.e., Kevlar29® layer first), 3) interfering layers (i.e., Spectra® layer first) and 4) all one material at the same areal density ratio. As seen in Figs. 4 and 5 compared with Fig. 3, the new version of the model gives results fairly consistent with the previous version [2], although the differences between interfering and noninterfering cases are significantly more pronounced with the new model, and the strains are slightly higher for the new model. The differences also increase markedly when the higher Spectra® modulus, 200 GPa, is used rather than 120 GPa. This means that the V_{50} velocity of penetration will differ widely when layer strains reach the failure strains. Additionally, using nondimensional time (normalized in terms of time $r_p/\hat{a}_{00}$ where $\hat{a}_{00}$ is an effective system tensile wave speed on impact) we see in Fig. 5 that the projectile velocity decay profiles are surprisingly very close among the various cases of coupling, despite the fact that the individual layer strains differ significantly.

Figure 6 shows results for the case of 12 layers each of Spectra® and Kevlar® (24 in total), thus allowing a higher impact velocity $V_p = 430$ m/s to achieve the same strain levels as in Fig. 5. Most striking is the fact that similar relative strain magnitudes are seen in Fig. 6 as compared with those in Fig. 5 except that difference in layer strains in the interfering case is even more pronounced in Fig. 6. Note

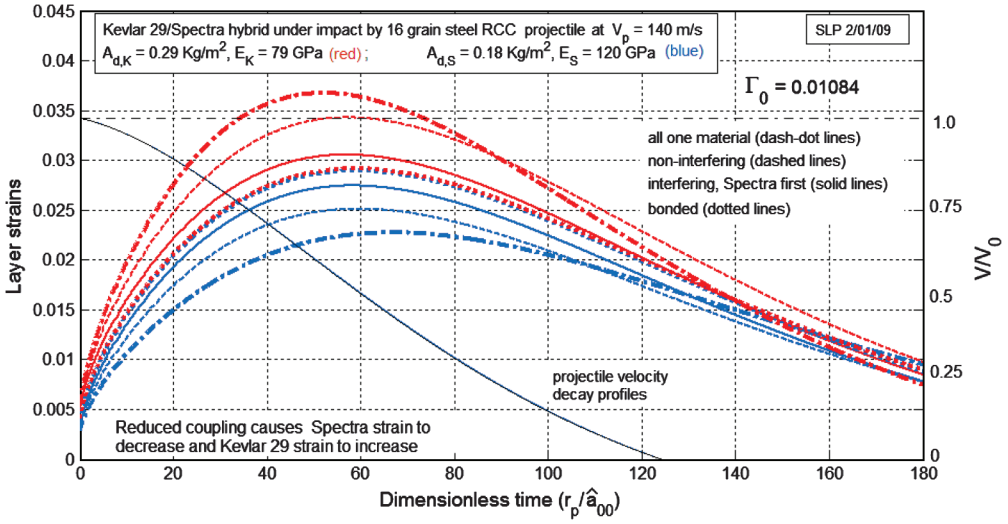

Fig. 4 Layer strain evolution predicted for the hybrid system of Cunniff [1] (assumed Spectra® modulus of 120 GPa) showing significant differences in strain patterns depending on the extent of layer coupling. Similar conditions to Fig. 3 at impact velocity 140 m/s.

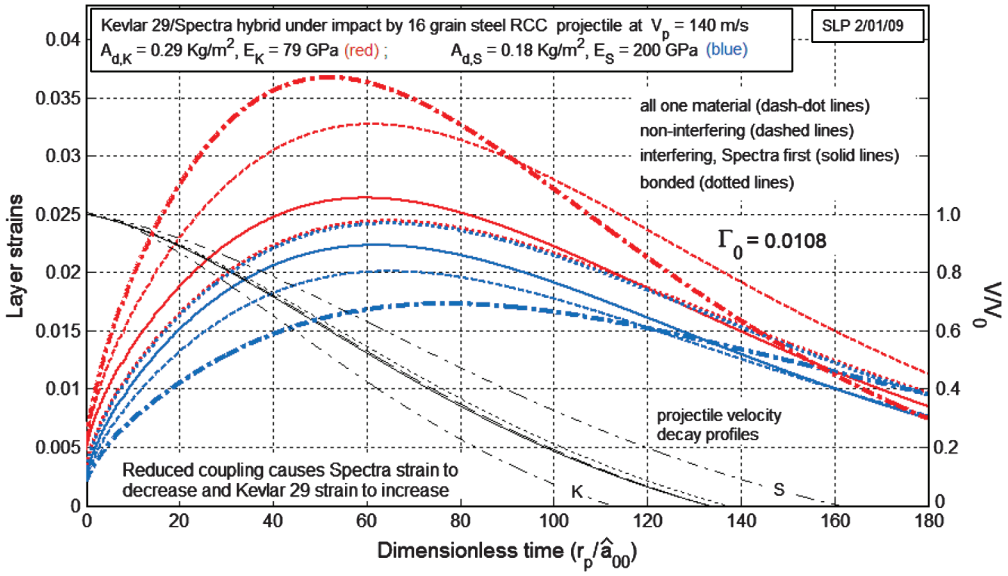

Fig. 5 Layer strain evolution predicted for experimental system of Cunniff [1] (Spectra® modulus of 200 GPa) showing much larger differences in strain patterns compared with those in Fig. 2, $V_p = 140$ m/s.

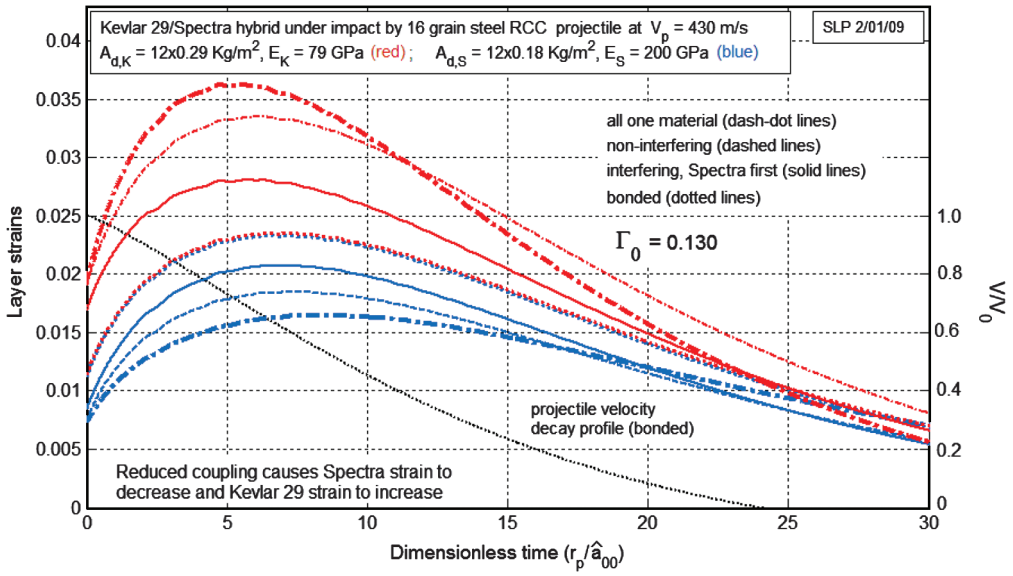

Fig. 6 Layer strain evolution predicted for system of Cunniff (assuming Spectra® modulus of 200 GPa) but with 12 layers each of Spectra® and Kevlar®, thus allowing a higher impact velocity of 430 m/s to achieve the same strain levels as in Fig. 5.

that the strain concentration is not as high by virtue of the whole deceleration process happening about a factor of 12 sooner in time despite the higher impact velocity. Based on Figs. 5 and 6 there is promise of effective scaling factors for similar systems but proportionally increasing numbers of layers.

VI. Conclusions

The most important result is that we were able to develop effective system properties for a hybrid system, allowing it to be largely expressed in terms of a single-layer problem and thus greatly simplifying the number of independent parameters needed, but allowing for detailed calculation of ply strains from the effective property solution depending on true material wave-speed ratios. Note that effective parameters are considerably different among cases of layers strongly bonded together versus interfering layers, noninterfering layers, and systems based on just one of the materials at the same overall fabric areal density.

Future work involves extending the model to stacked biaxial fabrics (orthotropic in plane with low shear modulus of similar materials with contrasting mechanical properties). Additionally we are treating the case of small air gaps between layers and the reduction in V_{50} velocity that results as the spacing increases.

Appendix A: Definition of Effective Quantities Immediately After Impact

Considering behavior immediately after impact we have $\varepsilon_{p,0,i} = \varepsilon_{c,0,i}$ so that the pulley analogy result gives

$$[c_{0,i}(1+\varepsilon_{p,0,i})]^2 = a_{0,i}\varepsilon_{p,0,i}\left[\frac{a_{0,1}\rho_1 h_1 + a_{0,2}\rho_2 h_2}{\rho_1 h_1/(1+\varepsilon_{p,0,1}) + \rho_2 h_2/(1+\varepsilon_{p,0,2})}\right] \quad i = 1,2 \tag{A1}$$

We consider the possibility of defining effective values right after impact as $\hat{c}_0$, $\hat{\varepsilon}_{p0}$, and $\hat{a}_{00}$ whereby we obtain a key mathematical relationship as occurs in the single-layer problem, that is

$$[\hat{c}_0(1+\hat{\varepsilon}_{p0})]^2 = \hat{a}_{00}\hat{\varepsilon}_{p0}\hat{a}_{00}(1+\hat{\varepsilon}_{p0}) \tag{A2}$$

By Eq. (15) in the main text we have $a_{0,1}\varepsilon_{p,0,1} = a_{0,2}\varepsilon_{p,0,2}$, and so we let

$$\hat{a}_{00}\hat{\varepsilon}_{p0} = a_{0,1}\varepsilon_{p,0,1} = a_{0,2}\varepsilon_{p,0,2} \tag{A3}$$

Also, because $c_1(1+\varepsilon_{p,0,1}) = c_2(1+\varepsilon_{p,0,2})$ right after impact we let

$$\hat{c}_0(1+\hat{\varepsilon}_{p0}) = c_1(1+\varepsilon_{p,0,1}) \tag{A4}$$

Finally we let

$$\hat{a}_{00}(1+\hat{\varepsilon}_{p0}) = \frac{a_{0,1}\rho_1 h_1 + a_{0,2}\rho_2 h_2}{\rho_1 h_1/(1+\varepsilon_{p,1}) + \rho_2 h_2/(1+\varepsilon_{p,2})} \tag{A5}$$

In order for this setup to provide effective quantities $\hat{a}_{00}$, $\hat{c}_0$, and $\hat{\varepsilon}_{p0}$, we must be able to solve for each of them uniquely. From Eqs. (A3) and (A5) we write

$$\hat{a}_{00} = \frac{a_{0,1}\rho_1 h_1 + a_{0,2}\rho_2 h_2}{\rho_1 h_1/(1+\varepsilon_{p,0,1}) + \rho_2 h_2/(1+\varepsilon_{p,0,2})} - \hat{a}_{00}\hat{\varepsilon}_0 = \frac{a_{0,1}\rho_1 h_1 + a_{0,2}\rho_2 h_2}{\rho_1 h_1/(1+\varepsilon_{p,0,1}) + \rho_2 h_2/(1+\varepsilon_{p,0,2})} - a_{0,1}\varepsilon_{p,01} \tag{A6}$$

and imposing a common denominator and using the fact that $a_{0,1}\varepsilon_{p,1} = a_{0,2}\varepsilon_{p,2}$ we can show

$$\hat{a}_{00} = \frac{a_{0,1}\rho_1 h_1 - a_{0,1}\varepsilon_{p,0,1}\rho_1 h_1/(1+\varepsilon_{p,0,1}) + a_{0,2}\rho_2 h_2 - a_{0,2}\varepsilon_{p,0,2}\rho_2 h_2/(1+\varepsilon_{p,0,2})}{\rho_1 h_1/(1+\varepsilon_{p,0,1}) + \rho_2 h_2/(1+\varepsilon_{p,0,2})} = \frac{a_{0,1}\rho_1 h_1/(1+\varepsilon_{p,0,1}) + a_{0,2}\rho_2 h_2/(1+\varepsilon_{p,0,2})}{\rho_1 h_1/(1+\varepsilon_{p,0,1}) + \rho_2 h_2/(1+\varepsilon_{p,0,2})} \tag{A7}$$

Then from Eqs. (A1) and (A3–A5) we confirm the validity of Eq. (A2) yielding the well-known form

$$\hat{c}_0 = \hat{a}_{00}\sqrt{\hat{\varepsilon}_{p0}/(1+\hat{\varepsilon}_{p0})} \tag{A8}$$

Then the layer strains, right after impact, are obtained as

$$\varepsilon_{p,0,i} = \hat{\varepsilon}_{p0}\hat{a}_{00}/a_{0,i}, \qquad i = 1,2 \tag{A9}$$

Appendix B: Definition of Effective Parameters at Intermediate and Long Times

We consider the development of effective properties to use the single-layer analysis to treat impact into two interfering layers. We recall Eq. (27) from the main text and despite convolution (time delay) effects and at extremely long time we eventually have $\varepsilon_{p,1}(t) \approx \varepsilon_{p,2}(t)$. From Eq. (27) and $\varepsilon_{c,i}(t) = \varepsilon_{p,i}(t)/r_{c,1}(t)$, we have

$$\frac{\varepsilon_{c,2}(t)}{\varepsilon_{c,1}(t)} \approx \left[\frac{r_{c,1}(t)}{r_{c,2}(t)}\right]\left[\frac{\ell n(1+t/t_{p,1})}{\ell n(1+t/t_{p,2})}\right] \tag{B1}$$

However, $r_{c,1}(t) \approx r_{c,2}(t)$ because $c_1(t)[1+\varepsilon_{c,1}(t)] \approx c_2(t)[1+\varepsilon_{c,2}(t)]$ and both $\varepsilon_{c,1}(t)$ and $\varepsilon_{c,2}(t)$ are small (well below the failure strains, which are <0.05) and actually approach each other in magnitude. Thus

$$\varepsilon_{c,2}(t)\,\ell n(1+t/t_{p,2}) \approx \varepsilon_{c,1}(t)\,\ell n(1+t/t_{p,1}) \tag{B2}$$

We recall a key result from the pulley analogy, Eq. (37), and desire to construct a similar effective structure. Define

$$\hat{c}(t)[1+\hat{\varepsilon}_c(t)] = c_1(t)[1+\varepsilon_{c,1}(t)] \tag{B3}$$

and

$$\hat{\varepsilon}_c(t) = \varepsilon_{c,1}(t)\frac{\ell n(1+a_{0,1}t/r_p)}{\ell n[1+\hat{a}_0(t)t/r_p]} \tag{B4}$$

as well as

$$\hat{a}_0^2(t)[1+\hat{\varepsilon}_c(t)] = \frac{\rho_1 h_1 a_{0,1}^2\left\{\frac{\ell n[1+\hat{a}_0(t)t/r_p]}{\ell n(1+a_{0,1}t/r_p)}\right\} + \rho_2 h_2 a_{0,2}^2\left\{\frac{\ell n[1+\hat{a}_0(t)t/r_p]}{\ell n(1+a_{0,2}t/r_p)}\right\}}{\rho_1 h_1/[1+\varepsilon_{c,1}(t)] + \rho_2 h_2/[1+\varepsilon_{c,2}(t)]} \tag{B5}$$

Thus, we have

$$\hat{a}_0^2(t) = \frac{\rho_1 h_1 a_{0,1}^2\left\{\frac{\ell n[1+\hat{a}_0(t)t/r_p]}{\ell n(1+a_{0,1}t/r_p)}\right\} + \rho_2 h_2 a_{0,2}^2\left\{\frac{\ell n[1+\hat{a}_0(t)t/r_p]}{\ell n(1+a_{0,2}t/r_p)}\right\}}{\rho_1 h_1[1+\hat{\varepsilon}_c(t)]/[1+\varepsilon_{c,1}(t)] + \rho_2 h_2[1+\hat{\varepsilon}_c(t)]/[1+\varepsilon_{c,2}(t)]} \tag{B6}$$

Using the fact that $\varepsilon_{c,1}(t)$, $\varepsilon_{c,2}(t)$, and $\hat{\varepsilon}_c(t)$ are all small, and recalling $t_{p,i} = r_p/a_{0,i}$, we can simplify Eq. (B6) to

$$\hat{a}_0(t) = a_{0,1}\sqrt{\frac{\ell n[1+\frac{\hat{a}_0(t)}{a_{0,1}}(\frac{t}{t_{p,1}})]\left\{\frac{\rho_1 h_1}{\ell n(1+t/t_{p,1})} + \frac{a_{0,2}^2}{a_{0,1}^2}\left[\frac{\rho_2 h_2}{\ell n(1+t/t_{p,2})}\right]\right\}}{\rho_1 h_1 + \rho_2 h_2}} \tag{B7}$$

Combining Eqs. (B3–B7) with a result from the pulley analogy, Eq. (37) leads to the desired form

$$\{(t)[1+\hat{\varepsilon}_c(t)]\}^2 = \hat{a}_0(t)\hat{\varepsilon}_c(t)\hat{a}_0(t)[1+\hat{\varepsilon}_c(t)] \tag{B8}$$

which yields the effective tensile wave speed (in unstretched material coordinates) as

$$\hat{c}(t) = \hat{a}_0(t)\sqrt{\hat{\varepsilon}_c(t)/[1+\hat{\varepsilon}_c(t)]} \tag{B9}$$

These two equations are of the same form as in the single-layer membrane impact problem. At very short times and long times, respectively, Eq. (B7) reduces to

$$\hat{a}_0(0) = \hat{a}_{00} \equiv \frac{a_{0,1}\rho_1 h_1 + a_{0,2}\rho_2 h_2}{\rho_1 h_1 + \rho_2 h_2} \tag{B10}$$

which is very close to Eq. (A7) when strains are small, and we obtain

$$\lim_{t\to\infty}\hat{a}_0(t) = \hat{a}_{0\infty} \equiv \sqrt{\frac{\rho_1 h_1 a_{0,1}^2 + \rho_2 h_2 a_{0,2}^2}{\rho_1 h_1 + \rho_2 h_2}} \tag{B11}$$

To evaluate the difference between Eqs. (B10) and (B11) we assume a fairly extreme but not unrealistic case where the two layers have equal thickness, $h = h_1 = h_2$, but material one is half as dense as material two, that is, $\rho_2 = 2\rho_1$. Also, the lighter material has a tensile wave speed $a_{0,1}$ twice as large as the other, $a_{0,1} = 2a_{0,2}$ (thus the lighter material also has double the stiffness). Using material one as the reference material, Eqs. (B10) and (B11) give the limits

$$\hat{a}_{00} = \frac{a_{0,1}\rho_1 h_1 + (1/2)a_{0,1}2\rho_1 h_1}{3\rho_1 h_1} = 0.6666a_{0,1}$$
$$\hat{a}_{0\infty} \equiv \sqrt{\frac{\rho_1 h_1 a_{0,1}^2 + 2\rho_1 h_1 a_{0,1}^2(1/4)}{3\rho_1 h_1}} = 0.7071a_{0,1} \tag{B12}$$

These limiting effective wave speeds differ by only 6%, despite the very large differences in layer properties.

Looking at an intermediate value, $t/t_{p,1} = 10$ closer to where the peak strain might be reached in the impact problem at moderate areal density ratio, Eq. (B7) yields

$$\frac{\hat{a}_0(t=10t_p)}{a_{0,1}} = 0.48170\sqrt{\ell n[1+10(\frac{\hat{a}_0(t)}{a_{0,1}})]} \tag{B13}$$

Substituting the two limits, $\hat{a}_{00}/a_{0,1} = 0.6666$ and $\hat{a}_{0\infty}/a_{0,1} = 0.7071$, into the right-hand side of Eq. (B13) gives $0.68748a_{0,1} < \hat{a}_0(t=10t_p) < 0.69609a_{0,1}$, which only differs by about 1.25%. Through iteration on Eq. (B7) we find that $\hat{a}_0(t=10t_p) = 0.69319a_{0,1}$. Because the lower bound differs from the correct value by less than 1% and yields the correct limits, we use this bound to calculate the effective tensile wave velocity $\hat{a}_0(t)$ at all times.

Thus, by choosing the appropriate parameter set the analysis for impact into a single membrane can treat the problem of impact into two interfering layers. The crucial quantity is the effective tensile wave speed taken as

$$\hat{a}_0(t) = a_{0,1}\sqrt{\frac{\ell n[1+\frac{\hat{a}_{00}}{a_{0,1}}(\frac{t}{t_{p,1}})]\{\frac{\rho_1 h_1}{\ell n(1+t/t_{p,1})} + (\frac{a_{0,2}}{a_{0,1}})^2[\frac{\rho_2 h_2}{\ell n(1+t/t_{p,2})}]\}}{\rho_1 h_1 + \rho_2 h_2}} \qquad t > 0^+ \tag{B14}$$

which right after impact gives Eq. (B10).

Appendix C: Cone Wave Front Position versus Strain History

We consider a single layer and recall Eqs. (50) and (57), but applied to a single layer. Substituting the latter into the former, taking the square root, multiplying both sides by $r_c(t)/r_p$, and cancelling common factors we obtain the instantaneous equation

$$\frac{c(t)}{r_p}\sqrt{\frac{r_c(t)}{r_p} + \varepsilon_p(t)} = \frac{a_0}{r_p}\sqrt{\varepsilon_p(t)} \tag{C1}$$

However, we also have the instantaneous result

$$\frac{\mathrm{d}}{\mathrm{d}t}\left[\frac{r_c(t)}{r_p} + \varepsilon_p(t)\right] = \frac{\mathrm{d}\varepsilon_p(t)}{\mathrm{d}t} + \frac{c(t)}{r_p} \tag{C2}$$

which can be written as

$$\frac{c(t)}{r_p}\,\mathrm{d}t = \left[\frac{r_c(t)}{r_p} + \varepsilon_p(t)\right] - \mathrm{d}\varepsilon_p(t) \tag{C3}$$

Thus, we can write

$$\sqrt{\frac{r_c(t)}{r_p} + \varepsilon_p(t)}\,\mathrm{d}\left[\frac{r_c(t)}{r_p} + \varepsilon_p(t)\right] = \frac{a_0}{r_p}\sqrt{\varepsilon_p(t)}\,\mathrm{d}t + \sqrt{\frac{r_c(t)}{r_p} + \varepsilon_p(t)}\,\mathrm{d}\varepsilon_p(t) \tag{C4}$$

or

$$\sqrt{\frac{r_c(t)}{r_p} + \varepsilon_p(t)}\,\mathrm{d}\left[\frac{r_c(t)}{r_p}\right] = \frac{a_0}{r_p}\sqrt{\varepsilon_p(t)}\,\mathrm{d}t \tag{C5}$$

Integrating both sides yields

$$\int_1^{r_c(t)/r_p} \sqrt{r_c(s)/r_p + \varepsilon_p(s)}\,\mathrm{d}[r_c(s)/r_p] = \frac{a_0}{r_p}\int_0^t \sqrt{\varepsilon_p(s)}\,\mathrm{d}s \tag{C6}$$

A crucial point is that $\varepsilon_p(t) \ll r_c(t)/r_p$ because $\varepsilon_p(t) \le \varepsilon_{p,\max} \ll 1$. In fact, as $\varepsilon_p(t)$ grows to $\varepsilon_{p,\max}$, $r_c(t)$ grows approximately in proportion. Thus, a good approximation in Eq. (C6) is to use $\varepsilon_p(s) = \varepsilon_{p,0}$ under the square root on the left-hand side. Thus, the left-hand side becomes

$$\begin{aligned}
&\int_1^{r_c(t)/r_p} \sqrt{r_c(s)/r_p + \varepsilon_{p,0}}\,\mathrm{d}[r_c(s)/r_p] \\
&\quad = \int_{1+\varepsilon_{p,\max}}^{r_c(t)/r_p+\varepsilon_{p,\max}} \sqrt{r_c(s)/r_p + \varepsilon_{p,0}}\,\mathrm{d}[r_c(s)/r_p + \varepsilon_{p,0}] \\
&\quad = \frac{2}{3}\left\{\left[\frac{r_c(t)}{r_p} + \varepsilon_{p,0}\right] - (1+\varepsilon_{p,0})^{3/2}\right\}
\end{aligned} \tag{C7}$$

Thus, from Eqs. (C6) and (C7) we have the simple result

$$\frac{2}{3}\left\{\left[\frac{r_c(t)}{r_p} + \varepsilon_{p,0}\right] - (1+\varepsilon_{p,0})^{3/2}\right\} = \frac{a_0}{r_p}\int_0^t \sqrt{\varepsilon_p(s)}\,\mathrm{d}s \tag{C8}$$

which rearranges to

$$\frac{r_c(t)}{r_p} = \left[\frac{3}{2}\frac{a_0}{r_p}\int_0^t \sqrt{\varepsilon_p(s)}\,\mathrm{d}\tau + (1+\varepsilon_{p,0})^{3/2}\right]^{2/3} - \varepsilon_{p,0} \tag{C9}$$

Acknowledgment

The authors wish to acknowledge the sponsorship provided by the U.S. Department of Justice through the National Institute of Justice under grant 2007-DE-BX-K003.

References

[1] Cunniff, P. M., "An Analysis of the System Effects in Woven Fabrics Under Ballistic Impact," *Textile Research Journal*, Vol. 62, No. 9, 1992, pp. 495–509.

[2] Porwal, P. K., and Phoenix, S. L., "Effects of Layer Stacking Order on the V50 Velocity of Two-Layered Hybrid Armor System," *Journal of Mechanics of Materials and Structures*, Vol. 3, No. 4, 2008, pp. 627–639.
doi:10.2140/jomms.2008.3.627

[3] Prevorsek, D. C., Chin, H. B., Kwon, Y. D., and Field, J. E., "Strain Rate Effects in Ultrastrong Polyethylene Fibers and Composites," *Journal of Applied Polymer Science: Applied Polymer Symposium*, Vol. 47, 1991, pp. 45–66.
doi:10.1002/app.1991.070470004

[4] Phoenix, S. L., and Porwal, P. K., "A New Membrane Model for the Ballistic Impact Response and V50 Performance of Multiply Fibrous System," *International Journal of Solids and Structures*, Vol. 40, No. 24, 2003, pp. 6723–6765.
doi:10.1016/S0020-7683(03)00329-9

[5] Porwal, P. K., and Phoenix, S. L., "Modeling of System Effects in Ballistic Impact into Multi-Layered Fibrous Structures for Soft Body Armors," *International Journal of Fracture*, Vol. 135, Nos. 1–4, 2005, pp. 219–251.

A. Palazotto
Associate Editor